Chemical Physics Impact 6 (2023) 100224

Contents lists available at ScienceDirect

Chemical Physics Impact

journal homepage: www.sciencedirect.com/journal/chemical-physics-impact

Adsorption mechanism of AsH_3 pollutant on metal-functionalized coronene $C_{24}H_{12}$-X (X = Mg, Al, K) quantum dots

Ernest C. Agwamba [a,c], Akaninyene D. Udoikono [a,b], Hitler Louis [a,b], Gideon E. Mathias [a,b], Innocent Benjamin [a,f,*], Onyinye J. Ikenyirimba [a], Daniel Etiese [a,b], Eze F. Ahuekwe [a,d], Amanda-Lee E. Manicum [e]

[a] Computational and Bio-Simulation Research Group, University of Calabar, Calabar, P.M.B 1115, Nigeria
[b] Department of Pure and Applied Chemistry, University of Calabar, Calabar, P.M.B 1115, Nigeria
[c] Department of Chemistry, Covenant University, Ota, Nigeria
[d] Department of Biological Sciences, Covenant University, Ota, Nigeria
[e] Department of Chemistry, Tshwane University of Technology Pretoria, South Africa
[f] Department of Microbiology, University of Calabar, Calabar, P.M.B 1115, Nigeria

ARTICLE INFO

Keywords:
Coronene QD
Quantum dot
Adsorption
Sensors
DFT

ABSTRACT

Inorganic arsenic compounds are frequently found to occur naturally or as a result of mining in soils, sediments, and groundwater. Organic arsenic exists mainly in fish, shellfish, and other aquatic life and as a result of this, it may be contaminated in edible consumables such as rice and poorly purified drinking water. Exposure to this toxic gas can cause severe lung and skin cancer as well as other related cancer cases. Therefore, the need to develop more efficient sensing/monitoring devices to signal or detect the presence of excessive accumulation of this gas in our atmosphere is highly demanding. This study has effectively employed quantum mechanical approach, utilizing density functional theory (DFT) to investigate the nanosensing efficacy of metal-decorated coronene quantum dot (QD); (Ca^{dec}QD, Al^{dec}QD, K^{dec}QD, and Mg^{dec}QD) surface towards the efficient trapping of AsH_3 gas molecule in an attempt to effectively detect the presence of the gas molecule which would help in reducing the health risk imposed by the AsH_3. The result obtained from the electronic studies reveals that the engineered molecules interacted more favorably at the gas and water phase than other solvents, owing to their varying calculated adsorption energies (E_{ads}). It was observed that the decoration of potassium and aluminum into the QD surface enhanced the adsorption process of AsH_3 gas onto K^{dec}QD and Al^{dec}QD surfaces with a comparably moderate level of stability exhibited by the said systems, which is evidently shown by the excellent energy gap (E_g) of 6.9599 eV and 7.3313 eV respectively for the aforementioned surfaces.

1. Introduction

Sensors are used in diverse industries and firms for military, health care, food processing as well as agriculture for several applications in a recent industrial landscape. The device that enhances the detection and transformation of a substance's quantifiable chemical, biological and physical qualities into human-readable signals are referred to as sensors. Ever since the discovery of nanosensors that operate on a nanoscale ($10^{-}9$ m), the use of traditional sensors has been limited due to the hypersensitivity of this nanoscale device. Carbon quantum dots (CQD) are a fast-metamorphosing new class of zero-dimensional carbon-based nanosystem (<10 nm) that has recently grown popular due to its outstanding sensing properties and has become of great importance after graphene, carbon materials, and carbon nanotubes. CQD have been reportedly observed to have the combined advantage of high conductivity, low purchasing cost, easy surface modification, high stability, low toxicity, and tunable photoluminescence (PL). As such the morphology of CQD is highly dependent on the method adopted for synthesis, which could influence the sensing property of the investigated CQD of interest. Nanomaterials employed to detect toxic gas include; metal oxide semiconductor gas sensors, nanotechnology-based medication delivery, and functionalized graphene quantum dots. Due to the uniqueness of these nanodevices owing to the closed electronic shells of its nanoclusters, functionalized quantum dot graphene has been reported to exhibit

* Corresponding author.
E-mail addresses: agwamba@covenantuniversity.edu.ng (E.C. Agwamba), innocentbenjamin@unical.edu.ng (I. Benjamin).

https://doi.org/10.1016/j.chphi.2023.100224
Received 12 January 2023; Received in revised form 17 April 2023; Accepted 6 May 2023
Available online 7 May 2023

outstanding physicochemical properties such as large surface area, high level of purity and stability, excellent electrical, optical, thermal, and catalytic properties as well as strong mechanical strength. The luminescence of carbon dotes was theoretically and experimentally investigated using the density functional theory approach by Yu et al. [1], as such it was observed that theoretical calculation and machine learning (ML) has become necessary to promote the development of the carbon dot photoluminescence (PL) field. For this to happen, there must be an improvement in the computing power and development of new theoretical methods which would play a more significant role and act as a guide to experiment [1]. 2D boron nitride materials as a sensor for H_2SiCl_2 were investigated by Mohsen Doust Mohammed et al. using the DFT approach. The result obtained from their study revealed that a decreasing trend of 5.742, 5.739, and 5.729 eV for boron nitride aluminum doped nanosheet ($BNAl^{dop}Ns$) was observed from the energy gap upon adsorption of dichlorosilane (DCS). These results obtained were observed to correlate strongly with the quantum theory of atoms in molecule (QTAIM) and adsorption studies for the aforementioned systems as gallium doped nanosheet ($BNGa^{dop}Ns$) exhibited comparably higher adsorption properties and sensitivity towards the detection of DCS gas than other studied doped surfaces [2]. Similarly, the interaction of water molecules to coronene and dodecabenzocoronene has been investigated and thus the result revealed that GDMA analysis of $C_{216}H_{36}$ acene as large as DBC gave a value of the carbon quadrupole moment nearly twice as large in magnitude as previously reported by the white house and Buckingham. However, the electrostatic and induction contributions due to the interaction of the water molecule with the carbon quadrupole moments are quite little at the minimum energy structure and thus is asserted that the water-graphite interaction energy (E_{int}) would be reduced in magnitude by only 0.1 kcal/mol. Thus, it was reported that their observation is in tandem with the findings of Bludsky et al. who used the DFT/CC approach to predict the interaction energy between water and a single graphite sheet where they obtained −2.8 kcal/mol E_{int} for a structure with water molecules situated slightly above the ring with both hydrogen atoms positioned down [3]. Also, the sensitivity of silver-graphene quantum dots for vital and harmful analytes was theoretically studied via the DFT approach by Tabish et al. [4]. After a detailed investigation, they further observed that the interaction energy of O_2@Ag-coronene (−61.06 kcal/mol) is the most stable molecule while NH_3@coronene is observed to exhibit the least stability of −4.00 $kcal.mol^{-1}$. As such, the order of interaction energy and percentage (%) reduction in HOMO-LUMO gaps were arranged in order of increasing stability as $O_2Ag_6 > NH_3@Ag_6 > C_2H_5OH@Ag_6 > H_2S@Ag_6$. Thus, silver-coronene composites are highly selective for the sensing of oxygen as seen to interact more favorably with silver clusters due to strong Ag….O electrostatic interactions [4]. Green synthesis of fluorescent CQD from eleusine coracana as well as its application as a fluorescence turn-off sensor probe for selective detection of Cu^{2+} was investigated using the DFT approach. The authors observed that Cu^{2+} preferentially got adsorbed on aromatic C-double bond C (π-bond) of CQDs whereas other divalent metal form σ – bond (s) with the CQDs, which is in tandem with the calculated HOMO-LUMO band gap and frontier molecular orbital analysis of the studied molecule [5]. Profoundly, AsH_3, a hazardous gas that is extremely reactive and poisonous, is a significant threat to both human health and the environment. A strategy for detoxifying AsH_3 from the environment that has evolved is its adsorption on functionalized quantum dots. Due to their distinctive electrical and structural characteristics, metal-functionalized coronene $C_{24}H_{12}$-X QDs, such as Mg, Al, and K, have been explored for their potential as AsH_3 adsorbents.

Descriptively, coronene ($C_{24}H_{12}$) is a polycyclic potent aromatic hydrocarbon carbon, and it is a well-known nanomaterial that is frequently employed at all scales. Due to its prominent and virtuosic components, including its exceptional stability in solar systems and mechanical, thermal, and conductive properties, this inestimable nanomaterial is widely used in a variety of sectors. Given the previously mentioned exceptional qualities of hexagonal crystalline coronene made from graphene, it has been shown that coronene can serve as bio-probes and has a significant role in biological studies such as DNA cleavage, charge-transporting, electroluminescent, sensing, and other varied applications [6]. Interestingly, the selected metals were chosen due to their unique chemical properties of forming oxides when exposed to air. These oxide layers can act as protective barriers against further oxidation, which helps to prevent corrosion of the underlying sensor surface. Secondly, these metals are abundant and low-cost., making them attractive choices for large-scale production. Interestingly, research has revealed that the selected metals are biocompatible, which implies they are suitable for use in medical and biological applications where the sensor surface may come into contact with living tissue [7,8]. Most researchers have recently been intrigued by the exceptional features of coronene to computationally examine the effectiveness of this nanostructure in trapping dangerous gases. Arsine (AsH_3) is a minute molecule that can easily percolate the human cellular respiratory tract thereby causing injury and death due to its alarming toxicity. Since arsenic is found to occur naturally in the environment through the biological activities of fungi and bacteria, most people are prone to easily contract this toxic gas by drinking water, breathing as well as food consumption [9]. Concurrently, in recent investigations, the adsorption mechanism and sensing of AsH_3, NH_3, and PH_3 on metal-functionalized materials have been investigated using density functional theory (DFT). For instance, Luo et al. [10] investigated the adsorption of AsH_3, NH_3, and PH_3 on graphene doped with rare-earth metals (REM=La, Ce, Nd, Pm, Sm, Eu, and Gd) using DFT calculations. They discovered that AsH_3, NH_3, and PH_3 molecules attach to the functionalized graphene's REM sites via their lone pair of electrons and that the adsorption energy increases as the concentration of REM does as well. Accordingly, their study revealed that the graphene in its purest form shows only weak physisorption to the gas molecules AsH_3, NH_3, and PH_3. However, their study projects that a significant amount of electron redistribution and orbital hybridization were also seen, as well as increased chemisorption toward NH_3 and PH_3 and decreased adsorption toward AsH_3. Similar to this, Mohammad Reza and co-workers [11] utilized DFT simulations to investigate the AsH_3 adsorption on pristine, P-doped, and Ga-doped graphenes. As the examined AsH_3 was unable to appreciably change the electrical characteristics of P-doped graphenes, they discovered that the adsorption energy of AsH_3 was higher on Ga-doped graphenes than on pristine and P-doped graphene. Perhaps, recent theoretical investigations on metal-functionalized nanomaterials have shown the potential of metal-functionalized nanostructures; quantum dots in gas sensing [12,13].

Hitherto, in this study, the interaction between the various metal-functionalized Coronene QD and ASH_3 will be investigated utilizing structural analysis, electronic properties, energy assay, et.Cetra. Thus, utilizing the density functional theory approach, the interaction between quantum dot $C_{24}H_{12}$- X encapsulated nanostructure, where X = Al, K, and Mg metals were investigated herein at the ώB97X-D/6-311++G (2d, 2p) level. This is why our interest is primarily centered on evaluating the sensing effectiveness of $C_{24}H_{12}$ metal-encapsulated nanoclusters on adsorbing arsenic gas. As such, this study evidently sought to explore the effects of the adsorption process on the electronic properties of metal-encapsulated $C_{24}H_{12}$ -X (X= Mg, Al, and K) nanoclusters to design a proper and effective chemical sensor.

2. Computational details

The density functional theory (DFT) method was used to predict the properties and chemical reactivity of the compound [14]. DFT is a quantum mechanical method used in sciences to predict the physical/chemical properties of atoms and molecules using functionals. The prediction of electronic properties of atoms/molecules is a product of the sum of the structure's external potential V_{ext} and the interelectronic effective potential V_{eff}.[1]. The ωB97XD [15] functional was utilized

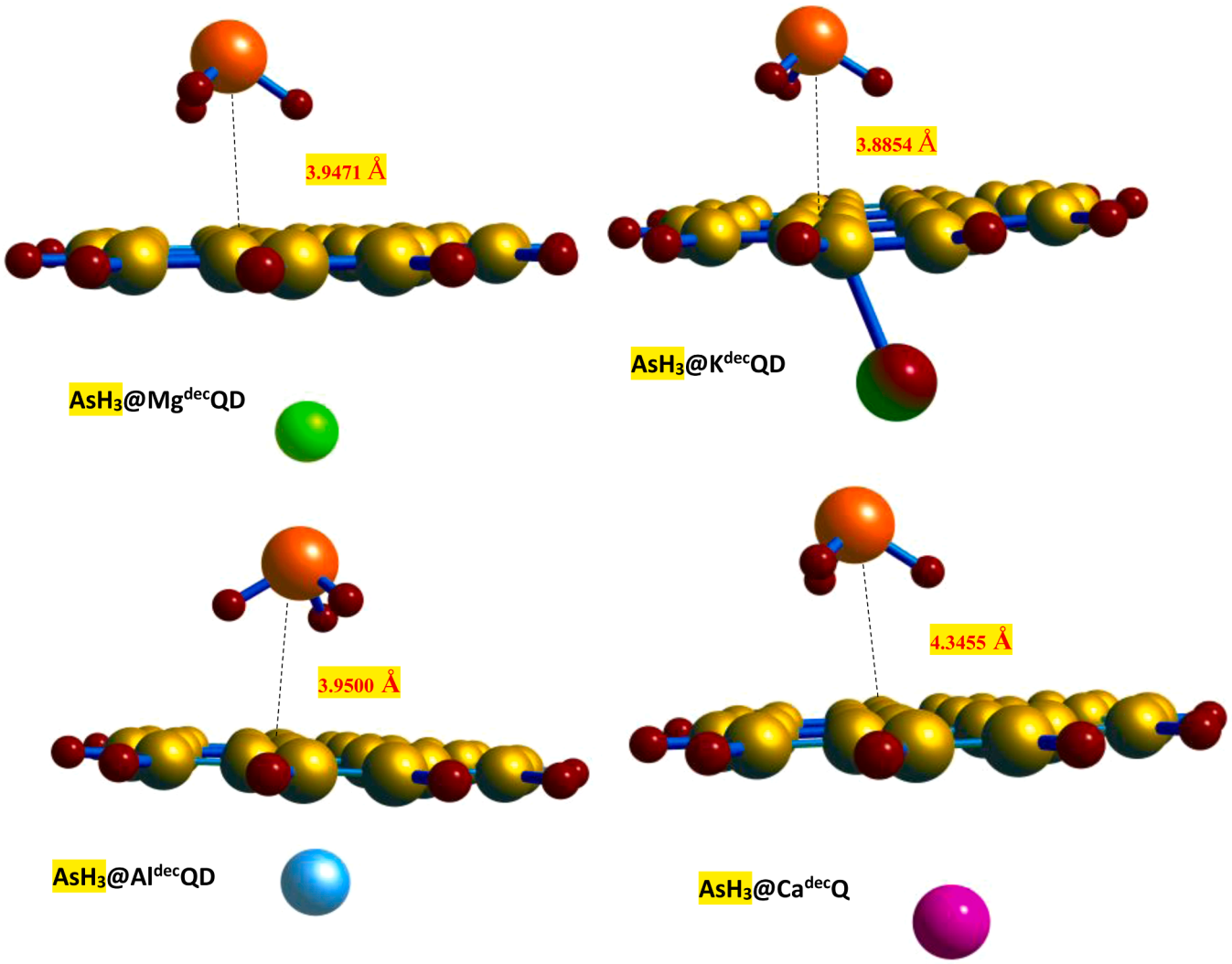

Fig. 1. Optimized geometric graphics of the studied compounds; adsorption configuration of AsH_3 on coronene QD surfaces calculated at ωB97XD/6-311 ++ G (2d,2p) level of theory.

together with 6-311 ++ G (2d 2p) [16] basis sets to optimize the compound. Gaussian 16 software [4] optimized and minimized the structure's energy. Natural bond orbital (NBO) analysis was calculated using NBO 3.1 module [16–19] embedded in the software. Non-linear optics (NLO) [20] was computed during the optimization process. Multiwfn 3.7[21]was used to calculate the DOS and QTAIM and GaussSum software [22] were also used to visualize the density of state (DOS) [23]. The frontier molecular orbitals (HOMO and LUMO) iso-surface visualization was carried out using Chemcraft [24]. Fig. 1 shows the optimized geometry of the adsorption configuration of AsH_3 on coronene QD surface calculated at ωB97XD/6-311 ++ G (2d,2p) level of theory.

3. Results and discussion

3.1. Geometry optimization

Substantially, the primary and most important phase in the computational investigation was to determine the optimal configuration of the metal-coated compound's interaction with arsine. It's worth noting that the ideal geometric parameters govern the orientation of each atom in the structure. In other words, bond lengths and bond angles were estimated with ωB97XD at the 6-311++ G(2d,2p) basis set as specified in, taking into account reactivity, phase of matter, polarity, and biological activity. A short bond length inside a compound results in a close bond between the elements that constitute the bond, making the molecule less reactive to other reactive species. As a result of the equivalence of the nitrogen and aluminum adsorption sites, the geometrical structure of the AsH_3@QD-X systems (X = Mg, K, Al, and Ca) exhibited a highly stable orientation. It is worth noting that the surfaces were strengthened during the optimization phase by sustaining a net charge of 0 (Q = 0 |e|) and duplet spin multiplicity (M = 2ST + 1 = 2) for K-decorated complexes and singlet multiplicity (M = 2ST + 1 = 1) for Mg, Ca, and Al-doped complexes. As compared to other systems, the system is composed of seven-membered rings with an adequate ratio of adsorption sites for the adsorption of any substance on its surface. The lengths of the Mg-C, K-C, Al-C, and Ca-C bonds vary with position, as reported in Table S1 of the supplementary information, and the adsorption geometries are illustrated in Fig. 1. In Table S1, it is seen that the bond lengths of Al-C all measured in are relatively short for the AsH_3@QD-X systems when compared to that of the QD-coated metals interaction with arsine; this suggests that AsH_3@QD-Al is less reactive than AsH_3@QD-Mg and AsH_3@QD-Ca, and this is consistent with the calculated quantum descriptors, particularly the energy gap, chemical softness (S) and electrophilicity (ω) [24]. Additionally, it is clear from the results that the bond length shortens as the bond angle shortens, which is consistent with the structural analysis. Likewise, the reactivity of QD increases with elements down the group and drops with elements across the period.

Table 1
Quantum chemical descriptors calculated at ωB97XD/6-311 ++ G (2d,2p) level of theory.

Quantum Descriptors	QD	AsH_3	$Mg^{dec}QD$	$K^{dec}QD$	$Al^{dec}QD$	$Ca^{dec}QD$	$AsH_3@Mg^{dec}QD$	A $sH_3@K^{dec}QD$	$AsH_3@Al^{dec}QD$	$AsH_3@Ca^{dec}QD$
E_{LUMO} (eV)	−0.1151	−0.6278	−0.0073	−0.2462	−0.2841	−0.2958	−0.2400	−0.2760	−0.3219	−0.3328
E_{HOMO} (eV)	−7.4274	−7.5967	−6.5313	−7.1941	−7.6176	−5.18323	−6.5533	−7.2361	−7.6532	−5.2058
IP(eV)	7.4274	7.5967	6.3313	7.1941	7.6176	5.18323	6.5533	7.2361	7.6532	5.2058
EA(eV)	0.1151	0.6278	0.0073	0.2462	0.2841	0.2958	0.2400	0.2760	0.3219	0.3328
Energy gap (eV)	7.3123	6.8789	6.3313	6.9478	7.3335	4.88743	6.3133	6.9599	7.3313	4.8730
χ (eV)	3.7713	4.0673	3.3657	3.7202	3.95085	2.73952	3.3967	3.7202	3.9508	2.7395
η (eV)	3.6562	3.4395	3.1656	3.4739	3.66676	2.44372	3.1566	3.4739	3.6668	2.4437
ω(eV)	1.9450	2.4048	2.1158	1.9919	2.12847	9.16997	1.8280	1.9919	2.1284	9.1699
S(eV)	0.2652	0.29074	0.3159	0.2878	0.27270	0.40920	0.3168	0.2879	0.2727	0.4092
μ(eV)	−3.7713	−4.0673	−3.3660	−3.7202	−3.9508	2.73952	−3.396	−3.7202	−3.9508	−2.7395
ΔE_n	−1.8281	−1.7197	−1.9095	−1.7369	−1.8333	−8.8563	−1.5789	−1.6413	2.1689	1.5737
ΔE_e	2.0621	3.0899	−4.1612	2.2468	−4.257	9.48363	2.0772	2.3145	9.8363	6.8023

3.2. Electronic properties

3.2.1. Frontier molecular orbital (FMO)

This study is tailored towards elucidating the relationship between adsorption energies of the investigated systems and their corresponding HOMO-LUMO band gaps prior and post adsorption onto arsenic molecule. The highest occupied and lowest unoccupied molecular orbital energy gap (HLEG) is observed to significantly influence the chemical reactivity of the studied compounds. Thus, energy gap (E_g) provides detail coherent on the extent of resistance to the change in the electron transfer of the investigated compounds [25]. Interactions (overlap) between an empty LUMO and a filled HOMO on one or more molecules can be optimally utilized to explicate resonance as well as reaction mechanism [26]. The frontier molecular orbital (FMO) hypothesis with respect to the resonance and reaction mechanism of a complex, sought to expatiate more on the morphology and reactivity of the studied compounds. In addition, FMO analysis seek to provide thorough explanation with respect to the stereo- and regioselectivities as well as other useful phenomena which is of great importance in studying the electronic behavior of the adsorbed systems. Thus, based on Koopmans theorem, the ionization energy, chemical softness, electron affinity, chemical potential and other parameters were calculated according to the following approximations [27]

$$I = -E_{HOMO} \tag{1}$$

$$I = -E_{LUMO} \tag{2}$$

$$\chi = -\mu = \frac{I + A}{2} \tag{3}$$

$$n = \frac{I - A}{2} \tag{4}$$

$$S = \frac{1}{2n} \tag{5}$$

$$\omega = \frac{\mu 2}{2n} \tag{6}$$

$$\Delta E_n = \frac{(\mu + n)2}{2n} \tag{7}$$

$$\Delta E_e = \frac{(\mu - n)2}{2n} \tag{8}$$

From Table 1 the energy gap reveals a slight distortion in the kinetic stability and interaction of the engineered surfaces, prior to and after adsorption. Quantum dot coronene (QD) was observed to exhibit energy gap of 7.3123 eV which was seen to decrease slightly with 0.981, 0.364, and 2.42487 eV upon encapsulation of Mg, K and Ca respectively. result show that when aluminum was encapsulated the efficacy of interaction and stability of the complex was enhanced with an increase of E_g = 0.0212 eV respectively. As such the highest kinetic stability was recorded when arsenide gas was adsorbed on $Al^{dec}QD$ which correspond to the high nucleofugality and electrofugality for the said molecule. Thus, this suggest that AsH_3@ $Al^{dec}QD$ system will easily adsorb the poisonous arsenide gas from AsH_3 molecule as a good nucleofuge and would separate itself from the substrate releasing an electron to nullify or inhibit the further release of AsH_3 gas to the environment as seen by electrofugality of 9.8363 eV and nucleofugality of 2.1689 eV for the aforementioned compound respectively. According to Marynard et al. and Parr et al. [28,29] a good electrophilic compound would possess a low (large negative) chemical potential (μ) value. As evidently seen, AsH_3@ $Mg^{dec}QD$, AsH_3@ $K^{dec}QD$, AsH_3@ $Al^{dec}QD$ and $AsH_3@Ca^{dec}QD$ follows the above decreasing trend with a corresponding (μ) of −3.3960, −3.7202, −3.9508 and −2.7395 eV respectively with a reduced chemical hardness of 3.1566, 3.4739, 3.6668 and 2.4437 eV for the aforementioned systems respectively. This implies that the studied molecules

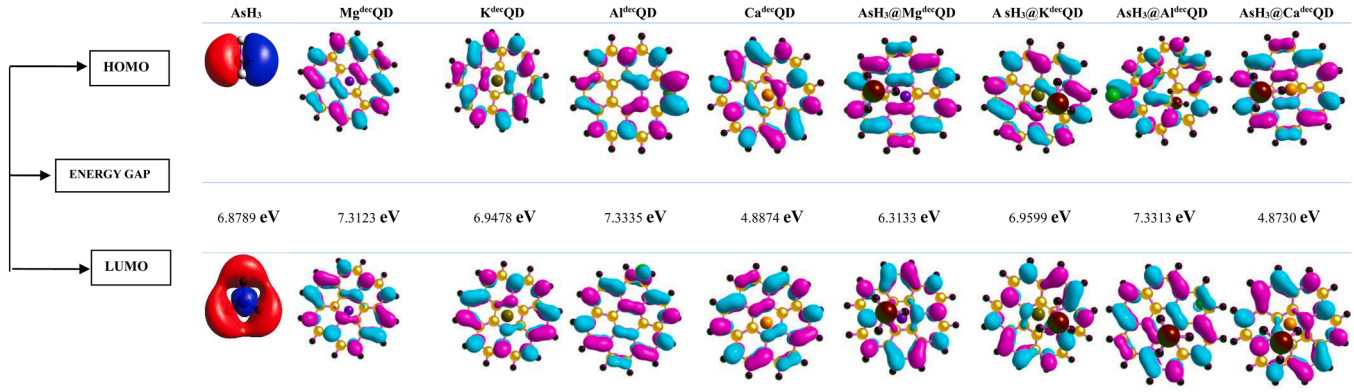

Fig. 2. HOMO, LUMO and energy gap differences of the optimized studied structures.

Table 2
NBO study of the quantum dot (QD) doped structures and interactions calculated at ωB97XD/6–311 ++ G (2d 2p) level of theory.

STRUCTURE	DONOR	ACCEPTOR	E(2)Kcal/mol	E(J)-E (I)	F(j)
QD	σH1-C3	π*C21-C27	307.40	0.04	0.110
	σH2-C4	π*C22-C28	182.06	0.06	0.104
	σC3-C4	σ*C10-C14	88.47	1.09	0.278
$Mg^{dec}QD$	σC_{27} - H_{31}	π^*C_{10} - C_{14}	151.08	0.28	0.194
	σC_{18} - C_{22}	π^*C_{10} - C_{14}	118.99	0.44	0.213
	σC_{18} - C_{22}	π^*C_{17} - C_{18}	49.68	1.35	0.233
$K^{dec}QD$	πC_{22} - C_{23}	π^*C_{13} - C_{19}	75.32	0.53	0.257
	πC_{13} - C_{19}	σ^*C_{20} - C_{24}	34.85	0.02	0.039
	σC_{18} - C_{22}	π^*C_{13} - C_{19}	30.45	0.98	0.250
$Al^{dec}QD$	σC_{21} - C_{27}	σ^*C_{21} - H_{25}	86.85	0.77	0.327
	σC_{17} - C_{21}	σ^*C_{21} - H_{25}	36.70	0.74	0.209
	σC_{17} - C_{18}	σ^*C_{21} - H_{25}	28.69	0.73	0.184
$Ca^{dec}QD$	πC_{19} - C_{20}	π^*C_9 - C_{13}	490.44	0.04	0.126
	π^*C_{24} - C_{29}	π^*C_{19} - C_{20}	337.66	0.01	0.110
	πC_{24} - H_{26}	π^*C_{10} - C_{14}	173.28	0.07	0.100
$AsH_3@Mg^{dec}QD$	σC_{10} - C_{14}	σ^*C_{20} - C_{24}	68.11	1.16	0.251
	σC_{14} – C_{20}	σ^*C_{20} - C_{24}	63.80	1.12	0.239
	πC_{17} – C_{18}	σ^*C_{19} – C_{23}	133.49	0.50	0.258
$AsH_3@K^{dec}QD$	σC18 – C22	σ*As37 – H38	54.91	0.96	0.292
	σC_{29} – C_{30}	σAs37 – H38	18.67	1.02	0.175
	πC8 – C11	σ*As37 – H39	116.00	42.79	8.943
$AsH_3@Al^{dec}QD$	π^*C_{24} – C_{29}	σ*C3 – C_7	31.17	0.74	0.551
	π*C24 – C_{29}	π^*C7 – C_{12}	77.30	0.54	0.458
	π^*C_{24} – C29	π^*C_{28} – C32	130.94	5.59	1.769
$AsH_3@QD^{dec}Ca$	π^*C_3 - C4	σ*As38 – H39	276.31	62.17	11.111
	π^*C_{10} – C_{20}	σ*As38 – H39	104.39	1.11	0.306
	σC_{19} – C_{20}	σ*As38 – H39	85.61	1.40	0.311

are in close agreement with Marynard et al. and Parr et al. theories as the studied systems obviously exhibit a good electrophilic property [30,31]. The lowest energy gap (E_g) is seen for $AsH_3@QD^{dec}Ca$ complexes depicting that $AsH_3@QD^{dec}Ca$ molecule is the least stable of all investigated compounds. Figure 2, illustrates the HOMO, LUMO isosurfaces of the studied systems. It is worth noting from the isosurface HOMO, LUMO mapping that the energetics of the system determines the distribution of the metal atoms (Mg, Al, K, or Ca) at the molecular center or edge in the AsH_3 pollutant adsorption mechanism on metal-functionalized coronene $C_{24}H_{12}$-X (X = Mg, Al, K) quantum dots. The AsH_3 pollutant's adsorption energy on the metal-functionalized coronene quantum dots can be affected by the location of the metal atoms. The AsH_3 pollutant molecule interacts with the surface of the quantum dot, releasing or absorbing energy in the process. Greater contact between the pollutant and the quantum dot is indicated by higher adsorption energy, which can improve the effectiveness of pollutant removal.

Generally speaking, the electronic characteristics of the metal atoms have an impact on the adsorption of molecules on metal-functionalized surfaces. The position of the metal atoms in the molecular structure can change their electronic characteristics, which can change the adsorption energy. Mg, K, and Ca are localized in the molecular center of metal-functionalized coronene quantum dots because they have a lower ionization potential and are more electropositive than Al. Due to their location in the molecular center and increased attractiveness to the AsH_3 pollutant, the metal atoms can interact with the pollutant molecule more successfully.

On the other hand, Al is distributed at the molecular edge because it has a higher ionization potential and is less electropositive than Mg, K, and Ca. This makes it less attractive to the AsH_3 pollutant, and its distribution at the molecular edge can help to shield the pollutant from the metal atom, reducing the interaction between the pollutant and the quantum dot. Overall, the distribution of the metal atoms in the molecular structure of the coronene quantum dots is determined by a balance of electronic and geometric factors that influence the adsorption energy and ultimately the pollutant removal efficiency.

3.2.2. Natural bond orbital analysis

The second-order Fock matrix was used in the NBO study to evaluate the interactions between the donors and recipients. The interactions lead to the localized NBO of the hypothetical Lewis structure losing its occupancy and becoming unoccupied in a non-Lewis orbital.[32]. For each donor I and acceptor (j), the stabilization energy $E^{(2)}$ associated with the delocalization i→j is computed as;

$$E^{(2)} = qi\frac{(F_{i,j})^2}{\varepsilon_j - \varepsilon_i} \tag{10}$$

where F(i, j) is the off-diagonal NBO Fock matrix member, εi and εj are diagonal elements, and *qi* is the *i*th donor orbital occupancy. The natural bond orbital analysis offers an efficient method for investigating intra- and intermolecular bonding and interaction among bonds, as well as a solid foundation for studying charge transfer or conjugative interaction in molecular systems. The second-order micro-disturbance theory was used to generate the interaction stabilization energy, which is what we report on along with a number of electron donors and acceptor orbitals. When the inclination for electron donors to donate to electron acceptors becomes stronger, the interaction between electron donors and acceptors intensifies, and the system has more conjugation overall leading to larger $E^{(2)}$ value. The delocalization of electron density between occupied Lewis-type (bond or lone pair) NBO orbitals and previously empty (antibonding or Rydberg) non-Lewis NBO orbitals leads to a stabilizing donor-acceptor interaction. The molecule has undergone NBO analysis to better understand the intramolecular, rehybridization, and delocalization of electron density which was carried out at the DFT/ωB97X-D/6311++G (2d, 2p) level of the theory as presented in Table 2.

The σ, σ*, π, and π* bond orbitals overlap between the carbons, hydrogens and metal groups forms an intramolecular interaction that results in intramolecular charge transfer (ICT) and stabilizes the system. These interactions cause the C—C antibonding orbital's electron density (ED) to increase, which weakens the associated bonds. The strong intramolecular hyper conjugation interaction between the and electrons of the C—C, C—H, M—C, and M—H bonds to the anti C—C, C—H, M—C, and M—H bonds stabilizes specific sections of the structures, as shown in Table 2. Comparing the stabilization energies of the four (metal-decorated) structures $Mg^{dec}QD$, $K^{dec}QD$, $Al^{dec}QD$, and $Ca^{dec}QD$), we observe that the highest stabilization energies of the intramolecular hyperconjugative interaction is between the σ, σ*, π, and π* C—C and C—H donor and acceptor orbitals. However, of the four doped structures, $Ca^{dec}QD$ displayed the most interaction energy, related to the resonance in the molecule between πC_{19} - C_{20} donor orbital and π^*C_9 - C_{13} acceptor orbital with a stabilization energy of 490.44 kcal/mol while $K^{dec}QD$ displayed the displayed minimal stabilization energy of 75.32 kcal/mol from the interaction between πC_{22} - C_{23} and π^*C_{13} - C_{19} donor-acceptor orbitals. The increase in the stabilization energies of the doped structures in the order; $Ca^{dec}QD > Mg^{dec}QD > Al^{dec}QD > K^{dec}QD$ comparing the stabilization energies of the interactions between the four (4) doped structures and arsine (AsH_3@ $Mg^{dec}QD$, $AsH_3@K^{dec}QD$, $AsH_3@Al^{dec}QD$, and $AsH_3@Ca^{dec}QD$), the highest interaction energy is observed between the πC_{17} – C_{18}, σ^*C_{19} – C_{23} and π^*C_{24} – C_{29}, π^*C_{28} – C32 donor-acceptor orbitals of $AsH_3@Mg^{dec}QD$ and $AsH_3@Al^{dec}QD$ with a stabilization energy of 133.49 and 130.94 kcal/mol while the minimal interaction energy is observed between the **σC_{18} – C_{22}** and **σ^*As_{37} – H_{38}** donor-acceptor orbitals of $AsH_3@K^{dec}QD$. The H—C interactions observed in $AsH_3@Al^{dec}QD$ donor and acceptor orbitals corresponds to the interaction between the hydrogens of arsine with the carbon of the

Table 3
QTAIM analysis of the QD-doped interactions.

Compound Structure	Bond	Bond Energy (kcal/mol)	ρ(r)	$\nabla^2\rho$ BCP	G(r)	K(r)	V(r)	H(r)	ELF	λ_1	λ_2	λ_3	$^{\varepsilon}$	λ_1 / λ_3
AsH_3@Ca^{dec}QD	Ca37-C18	−43.874	0.200	0.122	0.252	−0.539	−0.197	0.539	0.276	0.699	0.644	−0.120	−1.186	0.579
	H39-C23	−92.505	0.418	0.138	0.295	−0.512	−0.244	0.512	0.109	0.155	0.321	−0.196	−7.121	−0.041
AsH_3@K^{dec}QD	K41-C12	−26.696	0.123	0.559	0.122	−0.172	−0.105	0.172	0.232	−0.115	−0.931	0.663	7.083	0.081
	K41-C18	−43.204	0.197	0.112	0.237	−0.443	−0.192	0.443	0.298	0.624	0.616	−0.117	−1.189	0.507
	K41-C19	−63.059	0.286	−0.816	0.982	0.302	−0.400	−0.302	0.929	0.228	−0.554	−0.489	0.132	−0.261
	K41-C22	−63.728	0.289	−0.824	0.100	0.307	−0.407	−0.307	0.928	−0.558	0.221	−0.488	0.145	−0.07
	K41-C23	−68.635	0.311	−0.919	0.118	0.347	−0.465	−0.347	0.924	−0.610	0.215	−0.524	0.165	−0.086
	H38-C19	−139.352	0.628	0.186	0.408	−0.563	−0.351	0.563	0.221	−0.159	−0.319	0.205	4.008	−0.775
AsH_3@Mg^{dec}QD	Mg41-C18	−161.214	0.726	0.187	0.355	−0.115	−0.240	0.115	0.213	−0.256	−0.388	0.217	5.610	−1.179
	As37-C19.	−63.281	0.287	−0.834	0.963	0.305	−0.401	−0.305	0.933	−0.559	0.223	−0.499	0.121	−0.06
AsH_3@Al^{dec}QD	H40-C19	−129.090	0.582	0.175	0.382	−0.563	−0.326	0.563	0.195	−0.374	−0.136	0.193	2.630	−1.937
	Al41-C32	−60.159	0.273	−0.766	0.872	0.279	−0.366	−0.279	0.935	−0.523	0.229	−0.473	0.104	−0.05

quantum dot. However, of all the NBO interactions in the four structures, AsH_3@K^{dec}QD structure alone was stabilized by a metal (σ^*As_{37} – H_{39}) donor orbitals while the other three structures were stabilized mostly by σ, σ*, π, and π* C—C and C—H donor and acceptor orbitals. The increase in the stabilization energies of the four structures (AsH_3@Mg^{dec}QD, AsH_3@K^{dec}QD AsH_3@Al^{dec}QD, and AsH_3@Ca^{dec}QD) was observed in the order; AsH_3@Al^{dec}QD > AsH_3@Mg^{dec}QD > AsH_3@Ca^{dec}QD > AsH_3@K^{dec}QD. Potassium (K) displayed the least stabilization both in its doped structure and in interaction with arsine.

3.3. QTAIM analysis

Quantum theory of atoms in molecule (QTAIM) is an essential topological parameter as it provides crucial and vital information on the atomic and molecular interactions of bonds with respect to hydrogen bonding, owing to the fact that it is the easiest form of inter and intramolecular interactions within a system. QTAIM have been of great use to effectively categorize and summarize several assertions in the quantum theory of atoms in molecule (QTAIM). The topological parameters like the Hamiltonian kinetic energy K(r), electron density ($V_{\mathbf{Bcps}}$) and kinetic of electron density ($G_{\mathbf{Bcp}}$) have been carefully calculated in accordance to professor Richard F.W. Bader et al. theory [33]. According to Richard, the bond path identified within a compound are carefully positioned as pointers of a special pair-wise physical relationship within participating atoms. The concept of atoms in molecule (AIM) by Bader et al. helps to elucidate the nature of interaction within a molecular structure with respect to the bond critical points (Bcps) of a compound. As such the result from Table 3 expatiate that the binding (BE) between Al^{dec}QD, K^{dec}QD, Ca^{dec}QD and AsH_3 gas is −129.090, −139.352 and −92.505 kcal/mol for H_{40}-C_{19}, H_{38}-C_{19} and H_{39}-C_{23} Bcps while the visualization is presented in Fig. 3. Whereas, the binding energy for other intramolecular interactions within the investigated complexes were observed to vary from −43.874, −26.696, −43.204, to −63.059, −63.728, −68.635, −161.214 and −60.159 kcal/mol respectively. With respect to the obtained BE, it is evident that the surface interacted more favorably with the adsorbed gas owing to the high binding energy exhibited by the adsorbed molecules. So, to say, H_{40}-C_{19} bond critical points with BE of −129.090 and H_{38}-C_{19} Bcp with BE of −139.352 kcal/mol for AsH_3@Al^{dec}QD and AsH_3@K^{dec}QD molecules affirmed the excellent stability of the adsorbate and adsorbent upon adsorption which in agreement with the reactivity studies as well as adsorption studies for the aforementioned systems. Similarly, covalent interactions were observed between K_{41}-C_{19}, K_{41}-C_{22}, K_{41}-C_{23}, As_{37}-C_{19} and Al_{41}-C_{32} (BCPs) as shown from the negative Laplacian of electron density ($\nabla^2\rho$Bcp) while non-covalent interactions were observed for other inter and intramolecular interactions [34]. These elucidates that the adsorbed gas had a stronger interaction with the engineered surfaces which reflected at the parallel expansion (λ_1/λ_3) values, as they calculated λ_1/λ_3 for all studied molecules were observed to be less than 1. Notwithstanding, weak interactions were also recorded as shown from the positive Laplacian of electron density for few systems. According to several literature claims, we can evaluate the level of stability of a compound by first calculating the binding energy, since the stability of a molecule is directly proportional to the increment in binding energy. Studying the Ellipticity (ε) which is mathematically expressed as $\in = \lambda_1/\lambda_2 - 1$ where λ_1 and λ_2 designate the negativity of the Hessian of a system electron density at a given bond critical point. The order of ellipticity ($\in$) is thus arranged in accordance to decreasing preference as $\lambda_1 < \lambda_2 < 0 < \lambda_3$. Hence, it is asserted that the sensor surfaces exhibited a stronger hydrogen bond especially at H_{40}-C_{19}, H_{38}-C_{19} and H_{37}-C_{23} Bcps for AsH_3@Al^{dec}QD, AsH_3@K^{dec}QD and AsH_3@Ca^{dec}QD systems as shown in Table 3 [35].

3.4. Reduced density gradient

Reduced density gradient or non-covalent interactions (NCIs) are studied in order to better comprehend the diverse aspects of interactions, such as electrostatic interaction, π effect, van der waal forces, and hydrophobic effect [36]. RDG clusters, Reduced Density Gradient spikes, and λ2 all contribute to the RDG investigation by providing significant insight into the type of bond and the level of interaction [37]. The van der Waals interactions show values close to zero of λ2 and density ($\rho \approx 0$. $\lambda 2 \approx 0$), while the areas of strong repulsive interactions are known with a large positive of λ2 and high values of density ($\rho > 0$. $\lambda 2 > 0$) and hydrogen interactions show large negative values of λ2 with high values of density ($\rho > 0$. $\lambda 2 < 0$) [38]. The color-filled isosurface graphs were generated from the grid points using Visual Molecular Dynamics (VMD) software. There is absolutely no doubt that perhaps the

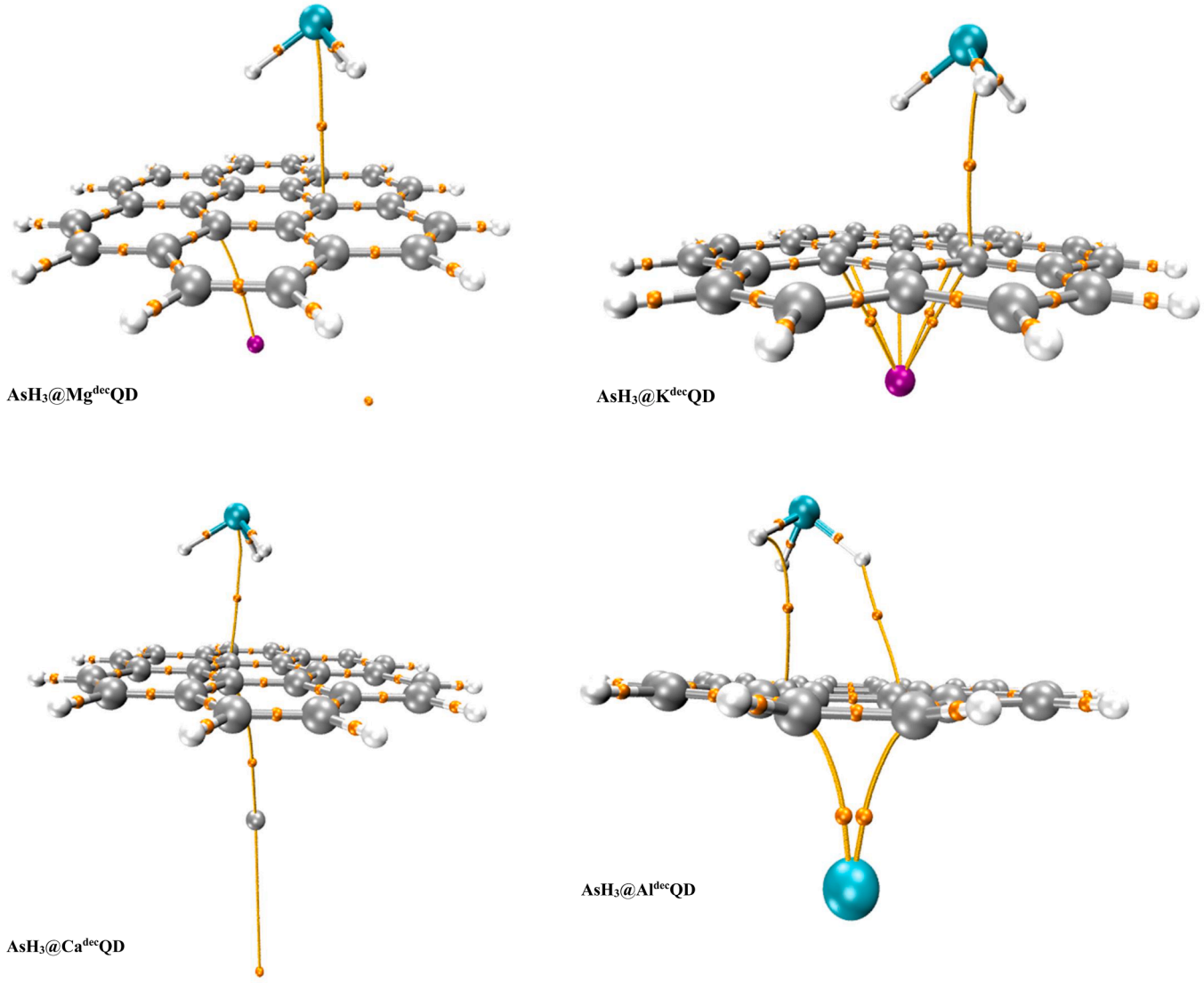

Fig. 3. QTAIM diagram of the interactions showing the bond critical points (Bcps) .

release of molecular energy, predominantly in the range of 1 to 5 kcal/mol (1000 to 5000 calories per 6.02 x 10^{23} molecules), occurs during the formation of NCI [39]. Figure 4 illustrates how the study is understood using a color palette with isosurfaces. The weak van der Waals dispersion interaction on the green isosurface explains the charge fluctuations that result in a unidirectional and non-specific attraction. The blue isosurface, on the other hand, exhibits a strong electrostatic force of interactions, which denotes the potential for hydrogen bond interaction and aids in the complexes' capacity to adhere to surfaces. Van der Waals force of interaction is illustrated by green isosurface. How to numerically solve for the decreased density gradient is shown in Eq. (11).

$$RDG = \frac{1}{2(3\pi^2)^{\frac{1}{3}}} \frac{|\overline{\Delta\rho}(\mathbf{r})|}{\overline{\rho(\mathbf{r})}^{\frac{4}{3}}} \tag{11}$$

The fact that the four complexes under investigation were virtually all subject to an apparent rather strong force of attraction as a result of the interactions between and within molecules is therefore intriguing to note. The deep blue color of $AsH_3@Al^{dec}QD$, $AsH_3@Ca^{dec}QD$, $AsH_3@Mg^{dec}QD$, and $AsH_3@K^{dec}QD$ suggests the existence of a very strong force of attraction resulting from hydrogen bond interaction, which facilitates the adsorption between the adsorption sites and the adsorbents. The emergence of peaks in the extraordinarily very negative zone of the eigen values provides further evidence that the aforementioned complexes exhibit a significant electrostatic force of attraction. Due to a lack of chemical bonds, these identical complexes were shown to exhibit physisorption. Significantly, connections at the real positive zones of the investigated complexes ($AsH_3@Al^{dec}QD$, $AsH_3@Ca^{dec}QD$, $AsH_3@Mg^{dec}QD$, and $AsH_3@K^{dec}QD$) that shimmer red, hence enhancing the instability of the interactions, demonstrate the existence of extremely mild steric repulsion. It is crucial to show that there is only very minor repulsion inside the doped surfaces, in contrast to the insignificant force of attraction and van der Waals interactions between these complexes. This is caused by the way that atoms are arranged spatially, which raises the energy in the surfaces. On the doped surfaces, which looked at less repulsive interactions, the nonbonding interactions had an impact on the conformation and reactivity of the ions. The structural groups of the surfaces' surfaces have overlapping electrons, which are kept in place by the way that like charges attract and opposite charges repel. $AsH_3@Al^{dec}QD$, $AsH_3@Ca^{dec}QD$, $AsH_3@Mg^{dec}QD$, and $AsH_3@K^{dec}QD$ was also evaluated for their comparatively high van der Waals form of contact, which suggests a little loss of equilibrium and an increase in the energy of adsorption between the molecules. The green color of the 3D RDG maps, however, indicates that practically all complexes have low van der Waals interactions.

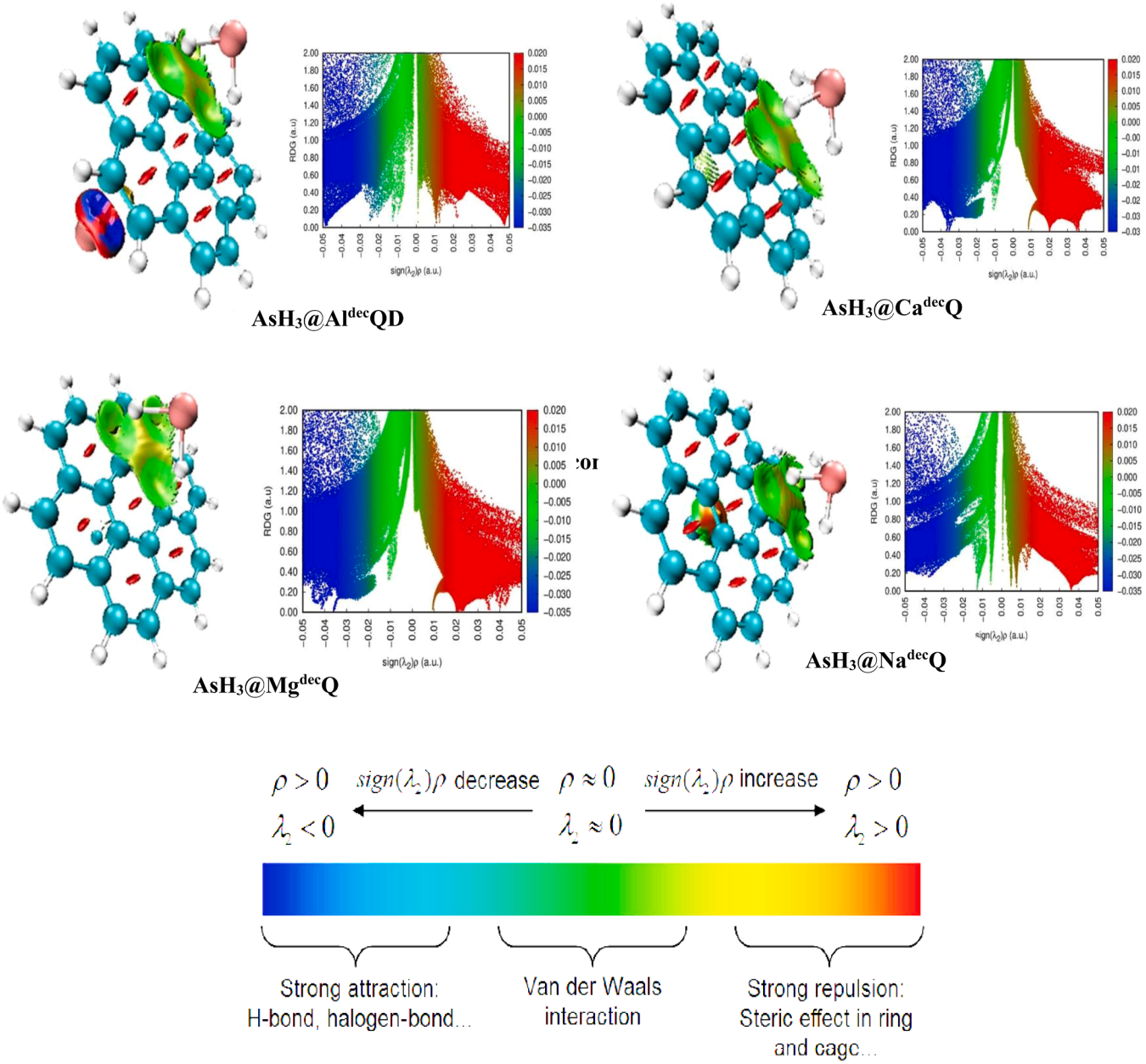

Fig. 4. Non covalent interaction plots for the studied systems.

3.5. Density of state (DOS) analysis

The density of states (DOS) of a molecule is seen as the number of states per energy interval at each energy level that are available to be filled or occupied by electrons. As such DOS theory lucidly describes electrons as roaming freely around and about the entire compound. However, DOS provides insight into the nature of discrete density distributions like spectra density possessed by the investigated surfaces. In addition, to effectually categorize the electronic structure of the studied systems, it is highly momentous and compelling to investigate the different density distribution within the adsorbed molecules as such Multiwfn and Origin softwares were exhaustively utilized for the DOS plot below. This is why our interest is tailored at examining the fragmental contribution of the adsorbate and adsorbent and how they tend to influence the stability of the investigated complexes at each energetic level as well as energy interval [40,41]. It is evident from Fig. 5 that aluminum and calcium fragment gave the highest contribution at the highest occupied molecular orbital (HOMO) from −1.0 to −0.30 eV for $AsH_3@Al^{dec}QD$ and $AsH_3@Ca^{dec}QD$ complexes, meanwhile magnesium and potassium fragment was observed to contribute passively from −0.75ev to −0.63 eV, −0.52 to −0.34 eV at the HOMO region for $AsH_3@Mg^{dec}QD$ and $AsH_3@K^{dec}QD$ molecules. Similar trend was also observed to occur at the LUMO region as Al and Ca fragment dominated from −0.32 to −0.10 eV energy interval for $AsH_3@Al^{dec}QD$ and $AsH_3@Ca^{dec}QD$ compounds, while the contribution of Mg and K remain minute at the LUMO region from −0.32 to −0.10 eV energy interval. Carbon and hydrogen fragment were further observed to give the maximum contribution at the HOMO region from −1.00 to −0.37 eV and −0.70 to −0.60 eV, −0.40 to −0.30 eV energy intervals for the pure surface (QD) and AsH_3 prior to decoration of cations and adsorption. The DOS plot at Fig. 5 reveals that, at the LUMO region, both Hydrogen and Arsenide contributed maximally from −0.30 to −0.25, −0.25 to −0.19 eV for AsH_3 gas. At the pure surface the DOS plot divulged that carbon fragment also participated conspicuously from −0.33 to −0.19 eV energy interval. Hence, the slight discrepancies observed by the fragments at the LUMO region for all studied compounds contributed to

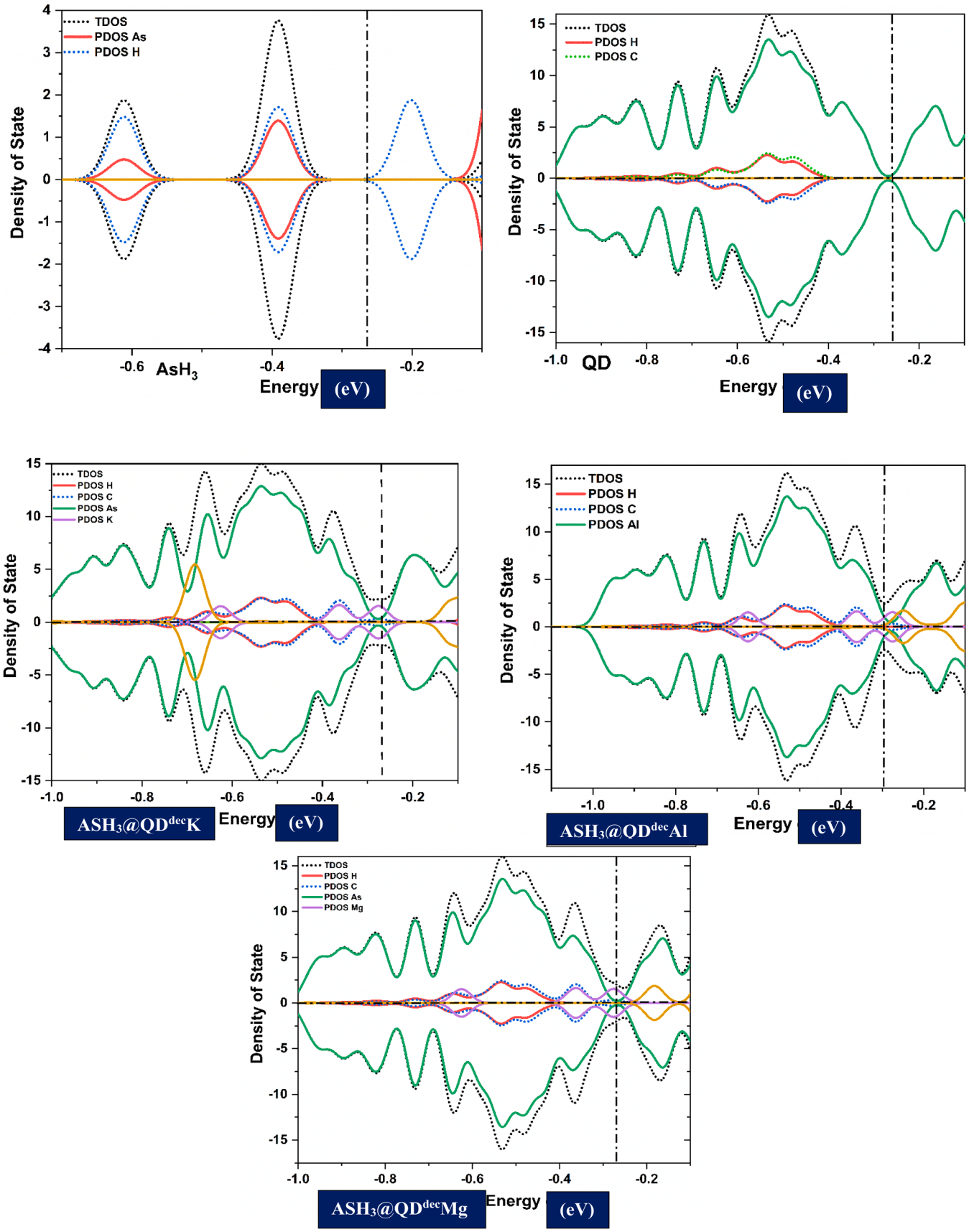

Fig. 5. Density of state plot of the decorated complexes.

Table 4
Adsorption energy (E_{ads}) in kcal/mol of the four systems in vacuum, benzene, ethanol and water after the adsorption of AsH_3 gas calculated at ωB97XD/6–311 ++ G (2d 2p) level of theory.

Structures	E_{ads} in Vacuum	E_{ads} in Benzene	E_{ads} in Ethanol	E_{ads} in H_2O
AsH_3@Mg^{dec}QD	−44.5206	−43.3559	−41.8838	−41.7601
AsH_3@K^{dec}QD	−44.8061	−43.6540	−41.9628	−41.8229
AsH_3@Al^{dec}QD	−44.7151	−43.5529	−42.1185	−41.9873
AsH_3@Ca^{dec}QD	−44.4879	−43.3019	−41.7325	−41.5317

the stability of AsH_3@ Al^{dec}QD and AsH_3@K^{dec}QD.

3.6. Electrochemical studies

The maximum amount of energy required to be delivered to the adsorbed atom in order to simplify the desorption process from a surface is referred to as the adsorption energy [E_{ads}]. Adsorption process is basically a surface based exothermic phenomenon that permits the disenthralling of large amount of energy when a gas is adsorbed onto a solid surface [42], with a corresponding decline in the residual forces acting on the surface of the adsorbent. The adsorption of AsH_3 on $QD^{dec}X$ where X = Mg, K, Ca and Al has been theoretically studied in different electronic medium like benzene, ethanol, water as well as in gas phase to meticulously grasp the adsorption mechanism, adsorption behavior and nature of interaction of the engineered surface with arsenide gas in each electronic medium respectively [43,44]. The reported adsorption energy for the investigated surfaces were calculated using density functional theory (DFT) at ωB97X-D3 hybridized dispersion correlation exchange functional employed to clearly capture every interaction between the adsorbate and the surface with little percentage error. 6–311++G(2d, 2p) basis set was employed to further appraise the computational accuracy. From Table 5, the calculated adsorption energies were observed to vary from gas to solvent phase. The E_{ads} for AsH_3@QD^{dec}Mg and AsH_3@QD^{dec}Ca at gas phase was observed to be −44.5206 and −44.4879 kcal/mol however, the highest E_{ads} was recorded for AsH_3@QD^{dec}K and AsH_3@QD^{dec}Al molecules at gas phase. As such a slight decreasing trend of −1.1647 and −1.186 kcal/mol was observed for the E_{ads} of AsH_3@QD^{dec}Mg and AsH_3@QD^{dec}Ca at benzene phase. The same trend was seen for AsH_3@QD^{dec}K and AsH_3@QD^{dec}Al compounds for the same phase. The lowest E_{ads} was observed when all systems interacted at water phase. More importantly, the highest adsorption energy was recorded for AsH_3@QD^{dec}K and AsH_3@QD^{dec}Al complexes which is observed to correlate strongly with the result obtained earlier from previous electronic studies of the modelled compounds. Thus, it is suspected that the nature of adsorption between the adsorbate and adsorbent is tilted towards chemisorption with respect to the high adsorption energies obtained as clearly tabulated in Table 5. However, the adsorption energies divulged that the engineered molecules interacted more favorably at gas phase than solvent, owing to their various calculated E_{ads} reported in Table 4. So, to say, the decoration of potassium and Aluminum onto quantum dot coronene (QD) enhanced the adsorption process of AsH_3 gas onto QD^{dec}K and QD^{dec}Al surfaces with comparably high level of stability exhibited by the said systems which is evidently shown by the excellent energy gap (E_g) of 6.9599 eV and 7.3313 eV for the aforementioned compounds. Thus, projecting QD^{dec}K and QD^{dec}Al surfaces as a promising potential sensor surface for AsH_3 gas.

3.7. Thermodynamics

The science concerned with the relations between heat and mechanical energy or work, as well as the conversion of one energy form to another is referred to as thermodynamics study. Thermodynamic study primarily centers on the relationship between large scale macroscopic properties like temperature, pressure as well as specific heat of a given system which can be ascertained by first considering the reaction mechanism of the isolated systems. The behavior of an isolated system is fathomed and accounted for by first studying the enthalpy (H), reaction entropy(S), heat capacity (Cv), free energy and volume (V) of the studied compounds with respect to first and second law of thermodynamics. In-depth knowledge of thermodynamic properties of an isolated molecule provides detail insight on the feasibility, direction r reaction pathway as well as time taken for the adsorption of AsH_3 gas on to metal decorated QD (Mg^{dec}QD Al^{dec}QD, K^{dec}QD and Ca^{dec}QD).

$$\Delta H^0(298K) = \sum \text{product}\Delta_f H^0\text{prod.}(298k) - - \sum \text{reactant}\Delta_f H^0\text{react.}(298k) \quad (12)$$

$$\Delta_f H^0(298K) = \sum \varepsilon_0 + H_{Corr}\text{product} - - \sum \varepsilon_0 + H_{Corr}(+)\text{reactant} \quad (13)$$

Where E_0 represent the electronic energy for both reactant and product species, H_{corr} designate the totality of electronic energy (EE) + thermal correction for both reactant and product species. The standard enthalpy of formation for product is symbolically represented as $\Delta_f H$, which is of great importance as it can be used to determine the nature of the adsorption process i.e. if the adsorption is endo or exothermic process. Thermodynamic parameters like electronic energy, entropy (S), thermal enthalpy correction as well as zero-point energy for the

Table 5
Thermodynamic properties for studied adsorptions calculated at ωB97XD/6–311 ++ G (2d 2p) level of theory.

Parameters	**Mg^{dec}QD**	**AsH_3**	**Product (AsH_3@Mg^{dec}QD)**
E_0	−1121.867226	−2237.625033	
E_{zpe}	0.282560	0.019700	
H_{corr}	−1121.567109	−2237.601472	
G_{corr}	−1121.632355	−223e7.602416	
$E_o + E_{ZpE}$	−1163.896047	−2237.605333	
$E_o + E_{tot}$	−2243.734452	−4475.250066	
$E_o + H_{corr}$	−2243.434335	−2237.602659	−4481.036994
$E_o + G_{corr}$	−2243.499581	−2237.628804	−4481.128385
$\Delta_f H^0$(298k)			−2237.767391 kcal/mol
ΔrG^0 (298k)			−2237.749143 kcal/mol
	K^{dec}QD	**AsH_3**	**Product (AsH_3@K^{dec}QD)**
E_0	−1521.725832	−2237.625033	
E_{zpe}	0.275811	0.019700	
H_{corr}	−1521.431669	−2237.601472	
G_{corr}	−1521.497606	−2237.602416	
$E_o + E_{ZpE}$	−1521.450021	−2237.605333	
$E_o + E_{tot}$	−3043.451664	−4475.250066	
$E_o + H_{corr}$	−3043.157501	−2237.602659	−5280.76016
$E_o + G_{corr}$	−3043.223438	−2237.628804	−5280.852242
$\Delta_f H^0$(298k)			- 2237.676295 kcal/mol
ΔrG^0 (298k)			−2237.751479 kcal/mol
	Al^{dec}QD	**AsH_3**	**Product (AsH_3@Al^{dec}QD)**
E_0	−1164.176678	−2237.625033	
E_{zpe}	0.280631	0.019700	
H_{corr}	−1163.878913	−2237.601472	
G_{corr}	−1163.939635	−2237.602416	
$E_o + E_{ZpE}$	−1163.896047	−2237.605333	
$E_o + E_{tot}$	−2328.353356	−4475.250066	
$E_o + H_{corr}$	−2328.055591	−2237.602659	−4565.65825
$E_o + G_{corr}$	−2328.116313	−2237.628804	−4565.745117
$\Delta_f H^0$(298k)			−2237.768161 kcal/mol.
ΔrG^0 (298k)			−2237.753125 kcal/mol.
	Ca^{dec}QD	**AsH_3**	**Product (AsH_3@Ca^{dec}QD)**
E_0	−921.803062	−2237.625033	
E_{zpe}	0.282326	0.019700	
H_{corr}	−921.505846	−2237.601472	
G_{corr}	−921.560457	−2237.602416	
$E_o + E_{ZpE}$	−921.520736	−2237.605333	
$E_o + E_{tot}$	−1843.606124	−4475.250066	
$E_o + H_{corr}$	−1843.308908	−2237.602659	−4080.911567
$E_o + G_{corr}$	−1843.363519	−2237.628804	−4080.992323
$\Delta_f H^0$(298k)			−3592.887484 kcal/mol
ΔrG^0 (298k)			−3592.876541 kcal/mol

Table 6
Calculated HOMO energies (E_{HOMO}), LUMO energies (E_{LUMO}), Fermi level energy (E_F), HOMO–LUMO energy gap (E_g), change in energy gap after AsH_3 adsorption (%Δ E_g), work function (Φ) and recovery time (τ) of the complexes after AsH_3 adsorption. Energies are in eV calculated at ωB97XD/6–311 ++ G (2d,2p) level of theory.

Structures	E_{HOMO}	E_{LUMO}	E_F	E_g	E_{ads}	Φ	τ
$Mg^{dec}QD$	−0.2309	−0.230	0.2309	0	–	−0.230	–
$K^{dec}QD$	−0.2455	−0.237	0.2414	0.00835	–	−0.241	–
$Al^{dec}QD$	−0.2498	−0.232	0.2411	0.01768	–	−0.241	–
$Ca^{dec}QD$	−0.2339	−0.233	0.2339	0.00001	–	−0.233	–
AsH_3@$Mg^{dec}QD$	−0.2309	−0.230	0.2309	0.00005	−44.520	−0.230	3.619 x 10^{-51}
AsH_3@$K^{dec}QD$	−0.2453	−0.237	0.2413	0.00818	−44.806	−0.241	2.241 x 10^{-51}
AsH_3@$Al^{dec}QD$	−0.2499	−0.232	0.2410	0.01779	−44.715	−0.241	2.611 x 10^{-51}
AsH_3@$Ca^{dec}QD$	−0.2309	−0.231	0.2309	0.00005	−44.487	−0.230	3.823 x 10^{-51}

adsorption process has been evaluated and reported in Table 5 for all sensor surfaces. It is observed that the standard enthalpy of formation Δ_fH^0 at constant temperature (298k) suggests that the adsorption process for all molecules is exothermic with an evolution of large amount of heat. As such the Δ_fH^0 for AsH_3@$Mg^{dec}QD$ and AsH_3@$K^{dec}QD$ is observed to be −2237.767391 and −2237.676295 kcal/mol. Meanwhile the Δ_fH^0 for AsH_3@$Al^{dec}QD$ and AsH_3@$Ca^{dec}QD$ is −2237.768161 and −3592.887484 kcal/mol. The Δ_fH^0 for AsH_3@$Mg^{dec}QD$ compound experienced a marginal decline upon decoration of K with a difference of 0.091096 kcal/mol. However, this infers that the adsorption of AsH_3 gas molecule by $Mg^{dec}QD$ surface is comparably more spontaneous than $K^{dec}QD$ sensor surface [45]. Nevertheless, the result explicates that the adsorption of AsH_3 gas on $Al^{dec}QD$ surface is feasible and spontaneous than $K^{dec}QD$ engineered surface owing to the theory which asserts that a spontaneous reaction is one in which the change in enthalpy of formation of the overall reaction process is negative. Thus, the decoration of Al and Ca on QD ($Al^{dec}QD$ and $Ca^{dec}QD$ a) lowers the activation barrier and appraised the spontaneous adsorption of AsH_3 gas. Result reveal that AsH_3@$Al^{dec}QD$ engineered sensor surface exhibited the most appreciable level of stability as seen from the adsorption and electronic studies of the complexes.

$$\Delta G^0(298K) = \sum \text{product}\, \Delta_r G^0 \text{prod.}(298k) - - \sum \text{reactant} \Delta_r G^0 \text{react.}(298k) \quad (14)$$

$$\Delta_r G^0(298K) = \sum (\varepsilon_0 + G_{Corr}) \text{product} - - \sum (\varepsilon_0 + G_{Corr}) \text{reactant} \quad (15)$$

The Gibbs free energy of a reaction in tandem with the standard enthalpy of formation helps to predict feasibility and spontaneity of a reaction. Thus, a spontaneous reaction is categorized by a negative Δ_rG^0 **i.e. (-Δ_rG^0 or** $\Delta G < 0$**)** while a spontaneous process can be fathomed by a positive Δ_rG^0. Based on the above established thermodynamic principle, the Δ_rG^0 at 298k for all studied molecules is in agreement with the standard enthalpy of formation (Δ_fH^0) at constant temperature (298 K), as both thermodynamic parameters evidently suggests that it is more feasible and spontaneous to adsorbed AsH_3 gas molecule using the modelled $Al^{dec}QD$ surface with respect to its excellent stability and effectual adsorption elucidated by the high E_{ads} exhibited by the said compound.

3.8. Sensing mechanism

In order to account for the sensitivity of the metal decorated quantum dot ($Mg^{dec}QD$, $K^{dec}QD$, $Al^{dec}QD$ and $Ca^{dec}QD$) towards AsH_3 gas their energy gap (E_g), and electrical conductivity (σ), were evaluated.

$$\sigma = AT^{3/2}e^{(-Eg/2kT)} \quad (16)$$

$$S = \frac{\frac{1}{\sigma gas} - \frac{1}{\sigma pure}}{\frac{1}{\sigma pure}} \quad (17)$$

Equation (16) gives the formula for determining the electrical conductivity (σ), of the sensor, where A is the Richardson constant, T is the working temperature (298 K) and k is the Boltzmann constant (2.0 × 10^{-3} kcal/mol.K). While Eq. (16) [45] gives the sensing response of the sensor where σ_{gas} and σ_{pure} are the conductivity of the doped quantum dot after and before adsorption. According to Eq. (16), the electrical conductivity of the adsorbent (decorated quantum dot) increases as the energy gap value decreases. From the results tabulated in Table 6, it can be seen that the adsorption of AsH_3 gas on the doped quantum dot affects their respective energy gap value. It was discovered that after the adsorption of AsH_3 the energy gap of $Mg^{dec}QD$, $Al^{dec}QD$ and $Ca^{dec}QD$ shifted from 6.3313 to 6.3133, 7.3335 to 7.3313 and 4.88743 to 4.8730 eV for all studied molecules respectively. However, the energy gap of $Al^{dec}QD$ was observed to decreased slightly after the adsorption of AsH_3 gas from 7.3335 eV to 7.3313 eV. This substantial change in E_g after the adsorption process influenced the electrical conductivity of the encapsulated quantum dot and this shows that the investigated structures hold a prospect to work as an electrochemical sensor to detect AsH_3. On the basis of Eqs. (3) and (4), the sensing response of the encapsulated quantum dot for AsH_3 gas are calculated to be 4.19 x 10^{-5}, −1.43 x 10^{-4}, 9.22 x 10^{-5}, and 3.36 x 10^{-5}, for $Mg^{dec}QD$, $K^{dec}QD$, $Al^{dec}QD$ and $Ca^{dec}QD$ respectively. Hence from the obtained result, it can be asserted that, $Al^{dec}QD$ and $Ca^{dec}QD$ engineered sensor surfaces possess a comparably better sensing efficiency for detecting AsH_3 gas molecule. The sensing response for the doped quantum dot follow the order $Al^{dec}QD > Mg^{dec}QD > Ca^{dec}QD > K^{dec}QD$. The strength of the interaction between the adsorbent and the adsorbate helps to evaluate the reusability of the gas sensor. The recovery time (τ) as shown in Eq. (18) is used to determine the time taken for the sensor to regain 90% of its original value after the removal of the detected gas. Shorter recovery time indicates a better performance of the sensor material.

$$\boldsymbol{\tau = A^{-1}e^{(-Eads/kT)}} \quad (18)$$

Where A, T, and k are the attempt frequency ($10^{12}s^{-1}$), test temperature, and Boltzmann's constant respectively. In this study, the test temperature is defined as 298 K. As such, the calculated recovery time, τ, of $Mg^{dec}QD$, $K^{dec}QD$, $Al^{dec}QD$ and $Ca^{dec}QD$ from AsH_3 are 3.619 x 10^{-51}s, 2.241 x 10^{-51}s, 2.611 x 10^{-51}s, and 3.823 x 10^{-51}s respectively [46]. These values indicate that our doped quantum dots have a short recovery and they all show a good prospect for detecting AsH_3.

3.9. Solvation assay

Solvation which is the process of applying a solvent to a chemical entity implicitly or explicitly has the ability to distorts the electron cloud of the said system due to electrostatic polarization interactions that affects the shape, energy and chemical activity of the system. Solvation energy gives the energy change associated with the transfer of a molecule between gas and solvent, it gives insight into how a chemical entity behaves in different environments. The stability of the doped quantum dot in the solvents is confirmed with the negative values for the solvation energies ($E_{solv.}$) which was calculated using equation (19);

$$E_{solv} = E_{T.sol.} - E_{gas} \quad (19)$$

Where the $E_{T.sol}$ represents the total energy of the system in the solvent

Table 7
Solvation energy of the referenced systems calculated at ωB97XD/6-311 ++ G (2d 2p) level of theory.

Structures	AsH_3	$Mg^{dec}QD$	$K^{dec}QD$	$Al^{dec}QD$	$Ca^{dec}QD$	$AsH_3@Mg^{dec}QD$	$AsH_3@K^{dec}QD$	$AsH_3@Al^{dec}QD$	$AsH_3@Ca^{dec}QD$
$E_{BENZENE}$	−1.258	−5.332	−12.096	−1.974	−8.151	−5.426	−12.202	−2.070	−8.224
$E_{ETHANOL}$	−2.733	−11.313	−26.587	−4.908	−17.816	−11.410	−26.477	−5.045	−17.794
E_{WATER}	−2.866	−11.851	−27.963	−5.218	−19.042	−11.956	−27.846	−5.356	−18.952

phase, and E_{gas} represents the total energy of the system in the gaseous phase [47]. The Solvation energy were calculated using the polarizable continuum model in benzene, ethanol and water for all doped quantum dots and the results are given in Table 7. From the results obtained the solvation energy of all the doped quantum dots increased on adsorption of AsH_3 except for $AsH_3@K^{dec}QD$ and $AsH_3@Ca^{dec}QD$ in ethanol and water. Despite the fact that the values obtained were all negative, a comparison of the predicted solvation energy values suggests that the systems are more stable in water than in other solvents [47].

4. Conclusions

The study utilized the hybrid dispersion correlation exchange (ωB97X-D3/6-311++G (2d, 2p)) level of theoretical of computation to carefully investigate the structural and electronic sensitivity of the engineered nanosensors towards adsorbing arsenide gas and the effect of encapsulating few selected cations (K, Al, Mg and Ca) on the quantum dot coronene (CQD) surfaces. Electronic properties of the adsorbed compounds such as adsorption energy, recovery time, topological analysis based on QTAIM, thermodynamic of adsorption, work function, natural bond orbitals as well as reactivity and conductivity studies were carried out to comprehend with certainty the effectiveness of the metal decorated quantum dot (QD) surafces ($Mg^{dec}QD$, $K^{dec}QD$, $Ca^{dec}QD$, and $Al^{dec}QD$) as nanosensors for AsH_3 gas. The obtained result divulged that the adsorbate molecule preferred to be trapped via the aromatic ring of $Al^{dec}QD$ and $K^{dec}QD$ surface. The electronic descriptor studies further affirmed the substantial stability of $Al^{dec}QD$ and $K^{dec}QD$ compounds which is observed to be in tandem with the adsorption studies of the said complexes. The decoration of cations especially K and Al enhanced the stability of the sensor surfaces, as QD surface is found to be more stable at energy gap (E_g) of 6.9599 and 7.3313 eV after interaction with AsH3 gas, which corresponds to the energy gap E_g obtained for $AsH_3@Al^{dec}QD$ and $AsH_3@K^{dec}QD$ surfaces. Prior to interaction, the E_g of $AsH_3@Al^{dec}QD$ and $AsH_3@QDK^{dec}$ systems were found to vary from 7.3335 eV, 6.94789 eV to 7.3313 and 6.9599 eV respectively. Thus, suggesting that the electrical conductivity of the quantum dot coronene nanosensor is appraised and will easily be converted to electrical signal. Also, the solvation studies explicated that all sensor surface interacted more effectively at water phase owing to their excellent solvation energies obtained. To further enhance the nature of adsorption between the adsorbate and adsorbent species, QTAIM topological analysis were conducted. Hence the obtained result reveal that the dominating stabilization interaction within the adsorbate and adsorbent is basically Vander Waals interaction without any steric hindrance observed within this region. The chemisorption adsorption nature of the systems was found to be strongly non-covalent with elevated binding energy exhibited at each bond critical points (BCPs) of intermolecular interaction. Thus $AsH_3@Al^{dec}QD$ and $AsH_3@K^{dec}QD$ modelled surfaces is proposed as a more efficient sensor material for detecting and adsorption of highly toxic AsH_3 gas molecule with little or no threat to the environment, health wise.

Data availability

All data generated or analyzed during this study are included within this article and its supporting information file

Authors contribution

Ernest C. Agwamba and **Hitler Louis**: Conceptualization, and supervision. **Akaninyene D. Udoikono, Gideon E. Mathias and Daniel Etiese**: Writing, Original draft, and Analysis. **Innocent Benjmamin and Onyinye J. Ikenyirimba**: Methodology, Investigation and writing. **Eze F. Ahuekwe and Amanda-Lee E. Manicum**: Resources.

Declaration of Competing Interest

The authors unanimously declare no financial or interpersonal competing interest.

Data availability

Data will be made available on request.

Funding

This work has not received funding from any agency or repository.

Acknowledgments

The center for high performance computing (CHPC), South Africa is gratefully acknowledged for providing computational resources for this project.

Supplementary materials

Supplementary material associated with this article can be found, in the online version, at doi:10.1016/j.chphi.2023.100224.

References

[1] J. Yu, X. Yong, Z. Tang, B. Yang, S. Lu, Theoretical understanding of structure –property relationships in luminescence of carbon dots, J. Phys. Chem. 12 (2021) 7671–7687.
[2] M.D. Mohammadi, H.Y. Abdullah, H. Louis, G.E. Mathias, 2D boron nitride material as a sensor for H2SiCl2, Comput. Theor. Chem. 1213 (2022), 113742.
[3] M. Rubeš, J. Kysilka, P. Nachtigall, O. Bludský, DFT/CC investigation of physical adsorption on a graphite (0001) surface, Phys. Chem. Chem. Phys. 12 (24) (2010) 6438–6444.
[4] A. Abbas, T.A. Tabish, S.J. Bull, T.M. Lim, A.N. Phan, High yield synthesis of graphene quantum dots from biomass waste as a highly selective probe for Fe3+ sensing, Sci. Rep. 10 (1) (2020) 1–16.
[5] T. Jadoon, T. Mahmood, K. Ayub, DFT study of silver-graphene quantum dots for vital and harmful analytes, J. Phys. Chem. Solids 153 (2021), 110028.
[6] E.N. Özmen, E. Kartal, M.B. Turan, A. Yazıcıoğlu, J.H. Niazi, A. Qureshi, Graphene and carbon nanotubes interfaced electrochemical nanobiosensors for the detection of SARS-CoV-2 (COVID-19) and other respiratory viral infections: a review, Mater. Sci. Eng. C 129 (2021), 112356.
[7] I. Obernberger, T. Brunner, G. Bärnthaler, Chemical properties of solid biofuels—significance and impact, Biomass Bioenergy 30 (11) (2006) 973–982.
[8] N. Deshwal, M.B. Singh, I. Bahadur, N. Kaushik, N.K. Kaushik, P. Singh, K. Kumari, A review on recent advancements on removal of harmful metal/metal ions using graphene oxide: experimental and theoretical approaches, Sci. Total Environ. 858 (2023), 159672.
[9] Wang Xi, P. Yang, Q. Feng, T. Meng, J. Wei, C. Xu, J. Han, Green preparation of fluorescent carbon quantum dot from cyanobacteria for biological imaging, J. Polym. 11 (4) (2019) 616.
[10] H. Luo, L. Zhang, S. Xu, M. Shi, W. Wu, K. Zhang, NH3, PH3 and AsH3 adsorption on alkaline earth metal (Be-Sr) doped graphenes: insights from DFT calculations, Appl. Surf. Sci. 537 (2021), 147542.

[11] M.R.P. Heravi, R.T. Kareem, P.D.K. Nezhad, A.G. Ebadi, S.M. Shoaei, S. Ahmadi, M. A. Jawad, AsH3 adsorption on pristine, P-doped and Ga-doped graphynes: a DFT Study, Bull. Mater. Sci. 45 (3) (2022) 107.
[12] A.N. Sosa, J.E. Santana, Á. Miranda, L.A. Pérez, A. Trejo, F. Salazar, M. Cruz-Irisson, NH3 capture and detection by metal-decorated germanene: a DFT study, J. Mater. Sci. 57 (18) (2022) 8516–8529.
[13] Y. Yu, C. Dai, DFT study of gas adsorption and sensing based on noble metal (Ag, Au and Pt) functionalized boron selenide nanosheets, Physica E Low-dimensional Syst. Nanostruct. 125 (2021), 114409.
[14] M. Malcek, M.N.D.S. Cordeiro, A DFT and QTAIM study of the adsorption of organic molecules over the copper-doped coronene and circumcoronene, J. Physica E Low-dimensional Syst. Nanostruct. 95 (2018) 59–70.
[15] V. Straskraba, R.E. Moran, Environmental occurrence and impacts of arsenide at gold mining sites in the western united states, Int. J. Mine Water 9 (1) (1990) 181–191.
[16] D. Bagayoko, Understanding density functional theory (DFT) and completing it in practice, AIP Adv. 4 (12) (2014), 127104.
[17] N. Mardirossian, M. Head-Gordon, $ω$B97X-V: a 10-parameter, range-separated hybrid, generalized gradient approximation density functional with nonlocal correlation, designed by a survival-of-the-fittest strategy, Phys. Chem. Chem. Phys. 16 (21) (2014) 9904–9924.
[18] H. Kjær, S.P.A Sauer, Pople style basis sets for the calculation of NMR spin–spin coupling constants: the 6-31G-J and 6-311G-J basis sets, J. Chem. Theory Comput. 7 (12) (2011) 4070–4076.
[19] Frisch, M.J.; Trucks, G.W.; Schlegel, H.B.; Scuseria, G.E.; Robb, M.A.; Cheeseman, J.R.; Scalmani, G.; Barone, V.; Petersson, G.A.; Nakatsuji, H.; et al. Gaussian 16 {R} evision {C}.01. 2016.
[20] F. Weinhold, C.R. Landis, E.D. Glendening, What is NBO analysis and how is it useful? Int. Rev. Phys. Chem. 35 (3) (2016) 399–440.
[21] F.S. Patrick-Inezi, W. Emori, H. Louis, C.G. Apebende, E.C. Agwamba, T. O. Unimuke, K. Wei, C.-.R. Cheng, V.M. Bassey, T.C. Egemonye, et al., Analeptic activity of 2-hydroxyl-5-nitrobenzaldehyde: experimental, DFT studies, and in silico molecular docking approach, Healthc. Anal. 2 (2022), 100030, https://doi.org/10.1016/j.health.2022.100030. January.
[22] Version, N. B. O. (1988). 3. Glendening, AE Reed, JE Carpenter, F. Weinhold; b) AE Reed, LA Curtiss, F. Weinhold. *Chem. Rev, 88*, 899.
[23] E.C. Agwamba, H. Louis, I. Benjamin, C.G. Apebende, T.O. Unimuke, (E)-2-((3-Nitrophenyl)Diazenyl)-3-Oxo-3-Phenylpropanal: experimental , DFT studies , and molecular docking investigations, Chem. Africa (2022), https://doi.org/10.1007/s42250-022-00468-4.
[24] T. Lu, F. Chen, Multiwfn: a multifunctional wavefunction analyzer, J. Comp. Chem 33 (5) (2012) 580–592.
[25] N.M. O'boyle, A.L. Tenderholt, K.M. Langner, cclib: A library for package-independent computational chemistry algorithms, J. Comput. Chem. 29 (5) (2008) 839–845.
[26] E.C. Agwamba, A.D. Udoikono, H. Louis, E.U. Udoh, I. Benjamin, A.T. Igbalagh, H. O. Edet, E.U. Ejiofor, U.B. Ushaka, Synthesis, characterization, DFT studies, and molecular modeling of azo dye derivatives as potential candidate for trypanosomiasis treatment, Chem. Phys. Impact 4 (2022), 100076, https://doi.org/10.1016/j.chphi.2022.100076.
[27] G.A. Zhurko, D.A. Zhurko, others, Chemcraft-Graphical Software for Visualization of Quantum Chemistry Computations, Ivanovo, Russ, 2016.
[28] K. Wei, H. Louis, W. Emori, P.S. Idante, E.C. Agwamba, C.-.R. Cheng, E.A. Eno, T. O. Unimuke, Antispasmodic activity of carnosic acid extracted from rosmarinus officinalis: isolation, spectroscopic characterization, DFT studies, and in silico molecular docking investigations, J. Mol. Struct. (2022), 132795, https://doi.org/10.1016/j.molstruc.2022.132795.
[29] A.D. Udoikono, H. Louis, E.A. Eno, E.C. Agwamba, T.O. Unimuke, A.T. Igbalagh, H. O. Edet, J.O. Odey, A.S. Adeyinka, Reactive azo compounds as a potential chemotherapy drugs in the treatment of malignant glioblastoma (GBM): experimental and theoretical studies, J. Photochem. Photobiol. 10 (2022) (2022), 100116, https://doi.org/10.1016/j.jpap.2022.100116.
[30] H. Louis, G.E. Mathias, O.J. Ikenyirimba, T.O. Unimuke, D. Etiese, A.S. Adeyinke, Metal-doped Al12N12X (X= Na, Mg, K) nanoclusters as nanosensors for corboplatin: insight from first-principles computation, J. Phys. Chem. B 126 (27) (2022) 5066–5080.
[31] A.T. Maynard, M. Huang, W.G. Rice, D.G. Covell, Reactivity of the HIV-1 nucleocapsid protein p7 zinc finger domains from the perspective of density-functional theory, Proc. Natl. Acad. Sci. 95 (20) (1998) 11578–11583.
[32] R.G. Parr, L.V. Szentpály, S. Liu, Electrophilicity index, J. Am. Chem. Soc. 121 (9) (1999) 1922–1924.
[33] P.W. Ayers, J.S.M. Anderson, L.J. Bartolotti, Perturbative perspectives on the chemical reaction prediction problem, Int. J. Quantum Chem. 101 (5) (2005) 520–534.
[34] G.I. Osigbemhe, E. Oyoita, H. Louis, E.M. Khan, E.E. Etim, H.O. Edet, O. J. Ikenyirimba, A.P. Oviawe, F. Obuye, Antibacteria potential of N-(2-furylmethylidene)-1,3,4-thiadiazole-2-amine: experimental and theoretical investigation, J. Indian Chem. Soc. 99 (9) (2022), 100597.
[35] E. Jaziri, H. Louis, C. Gharbi, T.O. Unimuke, E.C. Agwamba, G.E. Mathias, W. Fugita, C.B. Nasr, L. Khedhiri, Synthesis, X-ray crystallography, molecular electronic property investigation, and leukopoiesis activity of novel 4,6-dimethyl-1,6-dihydropyridin-2-amino nitrate hybrid material, J. Mol. Struct. 1268 (2022) (2022), 133733, https://doi.org/10.1016/j.molstruc.2022.133733.
[36] E.A. Eno, F.A. Patrick-Inezi, H. Louis, T.E. Gber, T.O. Unimuke, E.C. Agwamba, O. J. Ikenyirimba, J.A. Akpanke, E. Oyoita, E.U. Ejiofor, et al., Theoretical investigation and antineoplastic potential of Zn (II) and Pd (II) complexes of 6-Methylpyridine-2-carbaldehyde-N (4)-ethylthiosemicarbazone, Chem. Phys. Impact (2022), 100094, https://doi.org/10.1016/j.chphi.2022.100094.
[37] M.D. Mohammadi, F. Abbas, H. Louis, G.E. Mathias, Unimuke TO. Trapping of CO, CO2, H2S, NH3, NO, NO2, and SO2 by polyoxometalate compound, Comput. Theor. Chem. 1215 (2022), 113826.
[38] R. Padash, M.R. Esfahani, A.S. Rad, The Computational quantum mechanical study of sulfamide drug adsorption onto X12Y12 fullerene-like nanocages: detailed DFT and QTAIM investigations, J. Biomol. Struct. Dyn. 39 (15) (2021) 5427–5437.
[39] Hussain, S.; Hussain, R.; Mehboob, M.Y.; Ali, S.; Chatha, S.; Hussain, A.I.; Umar, A.; Khan, M.U.; Ahmed, M.; Adnan, M.; et al. Adsorption of phosgene gas on pristine and copper-decorated B12N12 nanocages: a comparative DFT study. 2020. https://doi.org/10.1021/acsomega.0c00507.
[40] Z. Rahmani, L. Edjlali, E. Vessally, A. Hosseinian, P. Delir Kheirollahi Nezhad, A DFT study on the sulfanilamide interaction with graphyne-like boron nitride nanosheet, J. Sulfur Chem. 41 (5) (2020) 483–497.
[41] H. Louis, O.J. Ikenyirimba, T.O. Unimuke, G.E. Mathias, T.E. Gber, A.S. Adeyinka, Electrocatalytic activity of metal encapsulated, doped and engineered fullerene-based nanostructured materials towards hydrogen evolution reaction, Sci. Rep. 12 (1) (2022) 1–21.
[42] S. Hussain, S.A.S. Chatha, A.I. Hussain, R. Hussain, M. Yasir Mehboob, A. Mansha, S. Nabel, K. Ayub, In Silico designing of Mg12O12 nanoclusters with a late transition metal for NO_2 adsorption: an efficient approach toward the development of NO_2 sensing materials, ACS Omega 6 (22) (2021) 14191–14199.
[43] M.R. Hossain, M.M. Hasan, S.U.D. Shamim, T. Ferdous, M.A. Hossain, F. Ahmed, First-principles study of the adsorption of chlormethine anticancer drug on C24, B12N12 and B12C6N6 nanocages, Comp. Theor. Chem. 1197 (2021), 113156.
[44] E. Nemati-Kande, R. Karimian, V. Goodarzi, E. Ghazizadeh, Feasibility of pristine, Al-doped and Ga-doped Boron Nitride nanotubes for detecting SF4 gas: a DFT, NBO and QTAIM investigation, App. Surf. Sci. 510 (2020), 145490.
[45] M.D. Mohammadi, F. Abbas, H. Louis, G.E. Mathias, T.O. Unimuke, Trapping of CO, CO2, H2S, NH3, NO, NO2, and SO2 by polyoxometalate compound, Comput. Theor. Chem. 1215 (2022), 113826.
[46] H. Liu, F. Wang, K. Hu, T. Li, Y. Yan, J. Li, The adsorption and sensing performances of Ir-modified MoS2 monolayer toward SF6 decomposition products: a DFT study, Nanomaterials 11 (1) (2021) 100.
[47] M.M. Kadhim, I. Waleed, Z.T. Abed, S.K. Hachim, S.A. Abdullaha, A.M. Rheima, DFT investigation for the adsorption of acrolein onto the surface of pristine and doped C70: NBO and QTAIM analyses, Comput. Theor. Chem. 1220 (2023), 113983.